2018 IEEE Intelligent Vehicles Symposium (IV)
Changshu, Suzhou, China, June 26-30, 2018

Path optimization for a wheel loader considering construction site terrain

Beichuan Hong[1,2] and Xiaoliang Ma[1,*]

***Abstract*—Wheel loader is one of the most widely used heavy-duty vehicles for transporting building materials in construction site. Improvement of its efficiency is important for sustainable transport and construction operations. This paper proposes a path optimization approach that allows us to plan loader trajectory and corresponding vehicle motions in construction site when the topological relief information is available. Vehicle dynamics is modeled for 3D motions considering the power balance of vehicle propulsion. The path planning problem is then formulated using a framework of constrained optimal control where vehicle dynamics is incorporated as system constraints. In order to solve the problem, a discrete search method is developed based on the principle of dynamic programming (DP), in which the states of the forward and backward movement paths of wheel loader are explored in parallel. A numerical study is then presented to demonstrate the application of the proposed approach for optimizing the loader path using terrain information.**

I. Introduction

Wheel loader is a type of heavy-duty vehicle that always conducts short-distance transport operations in construction project. The loading cycle consists of two moving procedures: a backward movement from the loading point to a reversing point and a forward movement from the reversing point to the unloading point, see Fig. 1. Such operations of wheel loader are an extensively repetitive task in most construction projects [1]. Therefore, the loading cycle can be automated and optimized for sustainable construction with respects to working efficiency, fuel consumption and environmental impacts.

Path planning techniques were applied to optimize the driving cycle of autonomous vehicles [2]. In [3], a graph-search algorithm was introduced to generate obstacle-avoiding trajectory for construction vehicles. The approach has an advantage in computational efficiency especially for complex driving environment. Meanwhile, in order to ensure the resulting path is curvature-continuous, Bźier and Clothoid curves were adopted to provide vehicle a feasible and smooth path [4], [5].

Different from path planning problem for onroad vehicles, wheel loader usually operates at a relatively closed environment with few complex driving scenarios. The optimization objectives of such repetitive loading tasks may include productivity, fuel efficiency and emissions. As a result, the methods concerning the power distribution of vehicle subsystems play an important role for planning loading trajectory [6], [7]. For example, optimal control approaches are applied for deriving loading path in [7], [8]. Our previous study [9] also proposed a discrete optimization approach that integrates vehicle dynamic models with a dynamic programming based approach. However, the loader model was simplified without considering the bucket position during the loading procedure. Meanwhile, the characteristics of the construction site are largely neglected. In real construction operations, wheel loader operates in a relatively small area but its performance could be significantly affected by its running patterns in construction site. The recent advancement of information and sensing technologies makes it possible to digitize the construction site using a wide spectrum of data collection methods such as laser scanning [10] and drones [11]. The prior knowledge about construction site such as terrain information can be used for path planning in construction projects.

This paper extends our early approach in [9] to optimize the loading operations in a known construction environment. Vehicle dynamic model is first introduced to characterize the power distribution during the loading operation and bucket height is explicitly modeled. A grid-based search algorithm is then established based on the DP approach while the terrain information is also considered. Compared to the early work, the computational efficiency is further improved by parallelizing the forward state exploration procedures for both backward and forward movements. The rest of the paper is organized as follows. Section II presents the model of wheel loader. The path optimization problem is presented in section III, where the optimization approach is also presented. A numerical study is finally carried out with some detailed analysis in section IV.

II. Vehicle system modeling

A. Vehicle dynamics

The dynamics of wheel loader can be described by an articulate kinematic model on the vehicle motion. In the model, (x, y) are the coordinate of vehicle location and z is the elevation of construction terrain. The motion of a construction vehicle is represented by

$$\dot{x} = v \cdot \cos\theta \cdot \cos\alpha \tag{1}$$

$$\dot{y} = v \cdot \sin\theta \cdot \cos\alpha \tag{2}$$

$$\dot{z} = v \cdot \sin\alpha \tag{3}$$

[1] Dept. of Civil and Architecture Engineering, KTH Royal Institute of Technology. Teknikringen 10, 10044, Stockholm, Sweden.
[2] School of Energy and Power Engineering, Wuhan University of Technology, Wuhan 430063, China.
This study is partly supported by the project "SCORE: Sustainable Construction Operations for Reduced Emissions" funded by Volvo CE.
* The corresponding author email: liang@kth.se.

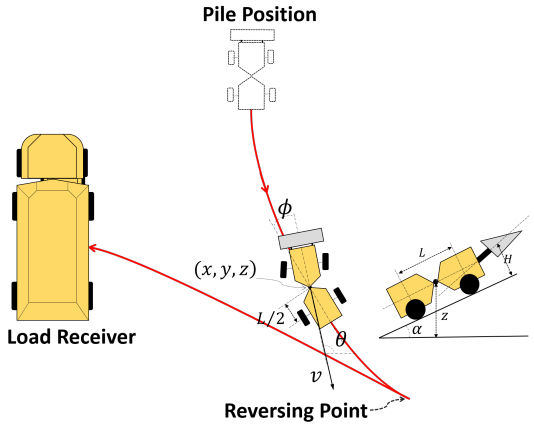

Figure 1. Trajectory of loading cycle: move backward to a reversing point and drive forward to receiver

where α is the slope gradient at (x, y), v is the velocity, and θ is the heading angle with respect to x-axis. The wheel loader is articulated vehicle with a pivot joint connecting the front and rear parts. The articulation angle ϕ, depicted in Fig. 1, can affect the vehicle steering performance as following:

$$\dot{\theta} = \frac{2}{L}.\ v.\ \cos\alpha.\ \tan\frac{\phi}{2} \tag{4}$$

$$\dot{v} = a \tag{5}$$

$$\dot{\phi} = \beta \tag{6}$$

where a is vehicle acceleration and steering angle β is the derivative of articulation angle which is controlled by wheel steering. L is the length between loader's front and rear wheels. Moreover, the turning radius and angular vehicle speed, respectively caculated by

$$R = \frac{L}{2\tan\phi/2} \tag{7}$$

$$\omega = \frac{v}{R} \tag{8}$$

are also limited by the geometric shape of the wheel loader to ensure continuous path curvature. Specifically, the boundary of control inputs a and β are determined by not only geometry limitation but the power distribution among vehicle propulsion system.

The propulsion system of a wheel loader consists of diesel engine, automatic transmission, hydraulic arm, drive shaft and so on. Table I summarizes the essential model parameters to describe the dynamics of the propulsion system during the loading process. The power usage of the wheel loader is modeled by the following equations:

$$P_{out} = P_{trac} + P_{str} + P_{lift} + P_{loss} \tag{9}$$

$$P_{trac} = v.\ m_{tot}.\ g.\ (c_r.\ \cos\alpha + \frac{v}{|v|}\sin\alpha + \frac{a}{g}) \tag{10}$$

$$P_{str} = c_p.\ \beta^2 \tag{11}$$

$$P_{lift} = \eta_l(H, n_e).\ m_{load}.\ g \tag{12}$$

$$P_{loss} = h(\frac{n_e}{v}, \gamma_d, T_e) \tag{13}$$

Table I
PROPULSION SYSTEM PARAMETERS

Parameter	Description
P_{str}	Power consumption for steering
P_{trac}	Power consumption for traction
P_{lift}	Power consumption for lifting system
P_{loss}	Power loss during loading process
P_e^{max}	Engine power upper band
T_e, n_e	Engine torque and speed
v, a	Vehicle speed and acceleration
θ, ω	Vehicle heading angle and its angular speed
ϕ, β	Articulation angle and steering angle
H	Height of loading bucket
$\gamma_g, \gamma_f, \gamma_{tc}$	Ratios of gearbox, differential, and torque converter
m_v, m_{load}	Loader weight, loading mass
m_{tat}	Equivalent total vehicle mass
r_w, α	Vehicle wheel radius, road slope
L	Length between vehicle front and rear axle

The engine output power P_{out} through loading operations is limited by "engine performance curve", which indicates the maximal engine power P_e^{max} determined by engine speed n_e. P_{trac} denotes the tractive power used for longitudinal rolling, climbing, and acceleration. Moreover, the lifting power P_{lift} is approximated by a polynomial function $\eta_l(H, n_e)$. The steering power P_{str} of wheel loader is proportional to the square of vehicle steering velocity according to [7]. Maps from the manufacturer are used for looking-up the values of P_{loss}. Coefficients c_p, c_r are used for power estimation.

The energy driving vehicle is constrained by the real-time power distribution in the propulsion system. Therefore, the vehicle motion is constrained as a result of power balance. Data from manufacturers are utilized to generate fuel consumption model $\psi(n_e, T_e)$ [9] depending on engine speed n_e (rad/s) and torque T_e (Nm). As the power source, the engine torque and the rotational speed can be derived as following:

$$T_e = \frac{P_{out}}{n_e} \tag{14}$$

$$n_e = \frac{\gamma_d.\ v}{r_w} \tag{15}$$

The $\gamma_d = \gamma_g\ \gamma_f\ \gamma_{tc}$ is total speed ratio of the driveline in which the torque converter ratio $\gamma_{tc} = g_{tc}(n_e/v, a)$ is defined by a looking-up table. In addition, brake specific fuel consumption (BSFC) is introduced to evaluate the fuel efficiency of the whole loading process. BSFC is the ratio of the total fuel consumption ψ divided by the sum of engine output power P_{out}, i.e.,

$$\delta(t) = \frac{\int \psi(n_e(t), T_e(t))dt}{\int P_{out}(t)dt} \tag{16}$$

B. State-space model

Geographical information has been widely available in construction site by remote sensing or other technologies [11]. This study assumes availability of the geographic information for the construction field. Thus, the terrain

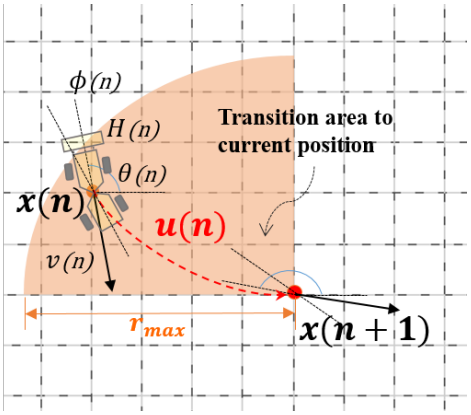

Figure 2. An example of state transition $\mathbf{x}(n) \rightarrow \mathbf{x}(n+1)$ during the backward procedure.

information is prior knowledge and can be represented as a uniform grid i.e. (x, y, z). In order to take advantages of the terrain information, the dynamics of wheel loader can be formulated as a discrete state-space model. Fig.2 describes the state transition of the loader while the vehicle state is expressed by

$$\mathbf{x} = [x \ y \ z \ v \ \theta \ \phi \ H]^T \tag{17}$$

where (x, y, z) marks the position of current state. The other variables in the state vector includes vehicle velocity, heading angle, articulation angle and bucket hight respectively. For each iteration, vehicle state evolves as follows:

$$\mathbf{x}(n+1) = F(\mathbf{x}(n), \mathbf{u}(n)) \quad \mathbf{u} \in \mathbf{U}(\mathbf{x}(n)) \tag{18}$$

where the control inputs are acceleration, the change of articulation angle and the variation of bucket height, i.e.

$$\mathbf{u} = [a, \beta, h]^T \tag{19}$$

Since the control input contains second-order derivative of vehicle state, the state transition between two grid nodes is approximated by a second-order Euler scheme:

$$\begin{aligned} x(n+1) =& x(n) + \Delta t(n) v(n) \cos\alpha(n) \cos\theta(n) \\ &+ \frac{1}{2}\Delta t(n)^2 \cos\alpha(n)[a(n)\cos\theta(n) \\ &- v(n)\sin\theta(n)\omega(n)] \end{aligned} \tag{20}$$

$$\begin{aligned} y(n+1) =& y(n) + \Delta t(n) v(n) \cos\alpha(n) \sin\theta(n) \\ &+ \frac{1}{2}\Delta t(n)^2 \cos\alpha(n)[a(n)\sin\theta(n) \\ &+ v(n)\cos\theta(n)\omega(n)] \end{aligned} \tag{21}$$

where the vehicle position (x, y, z) is given by terrain 3D map, then the ground slope α and angle velocity ω can be calculated by:

$$\alpha(n) = \arctan \frac{\Delta z(n)}{\sqrt{\Delta x(n)^2 + \Delta y(n)^2}} \tag{22}$$

$$\omega(n) = \frac{2}{L} v(n) \cos\alpha(n) \tan\frac{\phi(n)}{2}. \tag{23}$$

In a discretized grid, the time interval Δt for each state update can be calculated according to the state transition in (20) and (21). Then the transition of the other variables can be computed by:

$$\begin{aligned} v(n+1) &= v(n) + \Delta t(n) a(n) \cos\alpha(n) \\ \theta(n+1) &= \theta(n) + \Delta t(n) \frac{2}{L} v(n) \cos\alpha(n) \tan\frac{\phi(n)}{2} \\ \phi(n+1) &= \phi(n) + \Delta t(n) \beta(n) \\ H(n+1) &= H(n) + h(n) \end{aligned} \tag{24}$$

where discrete control input vector is $\mathbf{u}(n)$. Specially, the change of bucket hight $h(n)$ is simplified as a decision variable for switching among finite fixed state values. Finally, in order to satisfy the power balance according to the propulsion system model, the vehicle state, control inputs, and several internal variables are constrained in each iteration.

III. Path Optimization

A. Problem formulation

Our early work formulates the path optimization problem using a constrained optimal control framework [9]. The control objective is to minimize a cost-to-go function under certain constraints. It can be represented by

$$J(\mathbf{u}) = \int g\big(\mathbf{x}(t), \mathbf{u}(t)\big) dt \tag{25}$$

s.t.

$$\begin{aligned} \delta\big(\mathbf{x}(t), \mathbf{u}(t)\big) &\leq \bar{\delta}_{max} \\ T &\leq T_{max} \end{aligned}$$

where $g(\mathbf{x}(t), \mathbf{u}(t))$ is instantaneous cost function at time t, and $\mathbf{x}(t)$ is current system state controlled by $\mathbf{u}(t)$. Meanwhile, constants δ_{max} and T_{max} are set for constraining BSFC and time cost, respectively. Since the wheel loader model is high dimensional and nonlinear with non-convex objective function, the optimal control approach based on Pontryagin Minimum Principle (PMP) cannot easily handle the problem. This is even more difficult when the construction site terrain is involved.

In order to treat with the problem, a dynamic programming formulation is resorted. The approach may overcome the system nonlinearity and provide global optimization results. The idea leads to a DP recursion model on a spatial grid as follows:

$$\begin{aligned} J(n, \mathbf{x}_n) &= \min_{\mathbf{u}\in\mathbf{U}(n,\mathbf{x}_n)} \{g_n(\mathbf{x}_n, \mathbf{u})\Delta t_n + J(n+1, \mathbf{x}_{n+1})\} \\ & n = N-1, ..., 0 \end{aligned} \tag{26}$$

s.t.

$$\begin{aligned} \mathbf{x}_{n+1} &= \mathbf{f}(n, \mathbf{x}_n, \mathbf{u}_n); \ \mathbf{x}_n \in \mathbf{X}; \ \mathbf{u}_n \in \mathbf{U} \\ \sum \Delta t_n &\leq T_{max} \\ \delta_n &\leq \bar{\delta}_{max} \end{aligned}$$

where n is the iteration index, and the initial state $\mathbf{x}_0$ is given. $\mathbf{X}$ denotes the state space while the set of admissible control

variables $\mathbf{U}$ is determined by the current state $\mathbf{x}_n$. Noticeably, BSFC rate δ_n is instantaneously regulated by $\bar{\delta}_{max}$ for each step.

A conventional way to derive optimal vehicle trajectory is to solve a two point boundary value problem (BVP) with a fixed final state $\mathbf{x}(T) = \mathbf{x}_T$. However, the loading cycle for a wheel loader include a backward and forward procedure with the turning point unknown, and the conventional approach leads to tremendous computational cost in the experiment of [9]. Hence, we propose to handle the backward and forward movement in a parallel procedure in this work. For each movement, a DP model can be used to explore the optimal path.

B. Parallel searching

In this section, a search algorithm is developed to explore vehicle states based on the DP principle. For indexing simplification, a transformation is used to project the grid points of the work zone into an array with index p. This is illustrated in Fig 3 where the work zone, starting from p_o to p_b, portrays the space boundaries of the loading cycle. Without loss of generality, the wheel loader is assumed to have the ending position p_e at the left side of starting position p_s. The loading trajectory can be divided by a reversing point p_r connecting the backward and forward movement procedure. In addition, the areas for the backward and forward movement are marked by starting point p_s and ending point p_e. Hence, the wheel loader state vector at a position p can be expressed by

$$\mathbf{x}_p = [p \ v \ \theta \ \phi \ H]^T \tag{27}$$

where p is used as space index for the space-based recursion.

In contrast to the backward DP minimizing the cost-to-go function, the forward approach adopted maintains the cost-to-arrive $V(\mathbf{x})$ from initial state to the current. Since a wheel loader may have many potential states at a grid point, the state set $\mathbf{X}_p$ is introduced to represent all the possible vehicle states at position p. The forward recursion can generate new states based on the previous states. The whole process traverse the space by following the column-major order from the initial position (p_s or p_e) to the boundary p_b. The order of space-based iteration for backward movement procedure is in accordance with the motion sequence of the loader. In the forward movement procedure, the states are generated from the ending state till the potential reversing point.

In order to find the optimal reversing point p_r^*, the backward and forward searching procedures are carried out in parallel. Each procedure starts from the given initial state and the potential vehicle states are derived iteratively. $\mathbf{X}_p^b$ represents the set of potential states at position p derived in the backward movement procedure (from the initial point p_s). Similarly, for forward movement, $\mathbf{X}_p^f$ is generated from the final state at p_e. Note that b and f represent backward and forward procedures, respectively.

The recursion is a space-based state transition procedure that explores possible successors for known states. For a current position p, the search algorithm calculates the state $\mathbf{x}_p$ according to previous traversing states located inside the transition area Q_p, which is alread described by Fig.2. r_{max} denotes the maximum admissible distance between two continuous state in an iteration. The space-based recursion ends at the position p_b, the space boundary of the loading cycle.

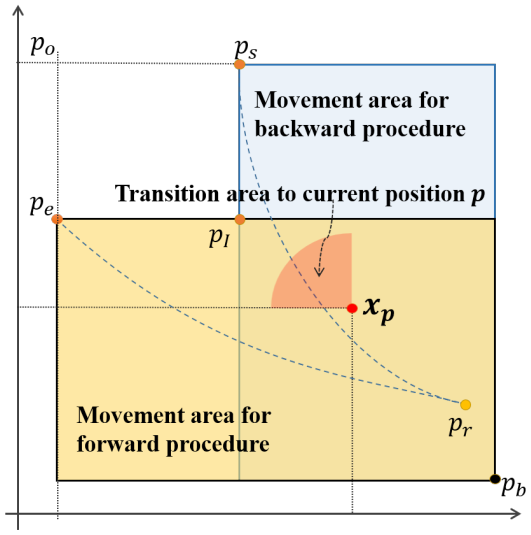

Figure 3. Illustration of the backward and forward procedures in the discretized working area. The point p_b represents the moving boundary specified by the construction scenario.

Starting from an initial position p_0 with a set of possible vehicle states $\mathbf{X}_p^0$, the algorithm for generating one moving procedure is listed as following:

1) **Define** vehicle moving area $\{p_0, p_1, ..., p_N\}$ by column-major-order. The last position is defined by the space boundary $p_N = p_b$ for both searching procedures.
2) **For** space-index p from p_1 to p_N **do**:
   a) *Determine* the transition area $\mathbf{Q}_p$ for position p defined by

$$\mathbf{Q}_p = \{q \in [p_1, ..., p] | d_{p,q} < r_{max};\ x_q < x_p;\ y_p < y_q\} \tag{28}$$

   where $d_{p,q}$ is the distance between q and p.
   b) *Calculate* the set of possible states $\mathbf{X}_p$

$$\mathbf{X}_p := \{\mathbf{x}_p | \mathbf{x}_p = f(\mathbf{x}_q, \mathbf{u}^*), \mathbf{x}_q \in \mathbf{X}_q, q \in \mathbf{Q}_p\} \tag{29}$$

   for each $\mathbf{x}_p \in \mathbf{X}_p$, there is an optimal control input $\mathbf{u}^*$ to minimize the cost-to-arrive $V(\mathbf{x}_p)$.

$$\begin{aligned} \mathbf{u}^* &= \underset{\mu(\mathbf{x}_p) \in \mathbf{U}(\mathbf{x}_q)}{\operatorname{argmin}} \{g(\mathbf{x}_q, \boldsymbol{\mu}(\mathbf{x}_p)) + V(\mathbf{x}_q)\} \\ V^*(\mathbf{x}_p) &= g(\mathbf{x}_q, \mathbf{u}^*) + V^*(\mathbf{x}_q) \end{aligned} \tag{30}$$

   where $g(\mathbf{x}_q, \mathbf{u}^*)$ is the running cost for state transition and $V^*(\mathbf{x}_p)$ is the optimal cost-to-arrive value for state $\mathbf{x}_p$.

The procedures are repeated for both backward and forward movements. The vehicle states are computed according to the space-index p, while the corresponding cost function $V(\mathbf{x})$ for each state is stored for later recovering the final optimal path.

C. Reversing point identification

After the potential states are explored, the next step is to identify the optimal reverse point so that an optimal path can be derived by connecting the two movement procedures. The intersection area, where reversing is possible, is outlined by $\{p_I, ..., p_b\}$. For each point inside the intersection area, we search the candidate state $\mathbf{x}$ that vehicle may change direction. The reversing candidate state $\mathbf{x}$ should be contained by both state sets, and only those states with speed close to zero are considered as candidates since hard braking leads to non-smooth driving and extra energy consumption. A criteria ε_v for justifying speed close to zero should be specified accroding the operation scenario. The algorithm for reversing point identification can be summarized by the procedures below:

1) **Define** the intersection area $\{p_I, ..., p_b\}$ and set initial value of optimal cost $J^*(\mathbf{x}) \leftarrow \infty$ for representing the sum of two cost-to-arrive function.
2) **Foreach** $p \in \{p_I, ..., p_b\}$ **do**:
   a) Find the states with zero speed shared by both backward and forward procedure:
   $$\mathbf{X}_p^r := \{\mathbf{x}_p | \mathbf{x}_p \in (\mathbf{X}_p^b \cap \mathbf{X}_p^f); v_p \leq \varepsilon_v\} \quad (31)$$
   b) Compute vehicle state $\mathbf{x}_p^*$ with minimal total cost:
   $$\mathbf{x}_p^* = \underset{\mathbf{x}_p \in \mathbf{X}_p^r}{\operatorname{argmin}} \{V^f(\mathbf{x}_p) + V^b(\mathbf{x}_p)\} \quad (32)$$
   $$J(\mathbf{x}_p^*) = V^f(\mathbf{x}_p^*) + V^b(\mathbf{x}_p^*) \quad (33)$$
   c) Update the minimal $J(\mathbf{x}_{p_r}^*)$ with corresponding vehicle state $\mathbf{x}_{p_r^*}$.

The optimal reversing point p_r^* is therefore obtained by minimizing $J(\mathbf{x}_{p_r}^*)$. Starting from the optimal reversing point, the final trajectory together with vehicle motion profile can be recovered from the state information stored before.

IV. Numerical Example

This section presents a numerical study on the optimization of the loading operation. The vehicle model uses the parameters of a LW321F prototype wheel loader, which was investigated in our early study [12]. Terrain spatial data were generated symbolically based on information from an example construction site. Fig. 4 outlines the working area of 16 m $\times$18m and the elevation ranges from 0 to 2.4m. The starting and ending positions of the loading cycle are fixed. Initial orientation of wheel loader is set to be $\theta = 90°$, in the direction toward the material pile.

Using our optimization approch, three different optimal trajectories are derived and shown in Fig. 5. Case a) is the optimal path computed using terrain information while the

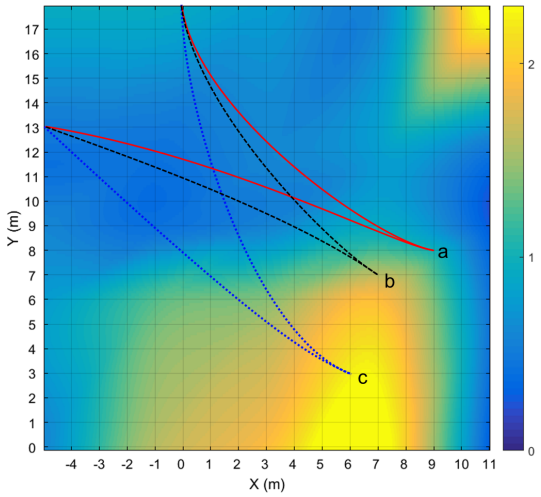

Figure 4. Illustration of optimal loading cycle trajectories: (a) a 3D path generated with operational lifting system; (b) a 3D path implemented with delay lifting strategy; (c) a 2D path optimized without considering terrain information. The starting position is $(0, 0, 0)$, and the ending point for the loading cycle is fixed at $(-5, 13, 0)$.

operation of lifting system is modeled during the loading process. Case b) implements a delay lifting strategy i.e. the lifting system doesn't conduct any operation until the loader arrives at the unloading point. Such a strategy is to handle the problem that the lifting bucket disturbs the vision of a human operator. In case c), the path is generated without taking into account terrain information in the optimization process and the ground level is assumed to be completely flat. Such a path is used by the loader to run on the terrain same as in case a) and b).

The simulation gives different optimal paths for three cases in Fig. 5. In both case a) and b), the wheel loader chooses to avoid the ground slop with relatively sharp steering while terrain information is considered. Due to the wheel loader's articulated structure both vehicle speed v and articulation angle ϕ are rapidly increased to steer the heading angle θ. Hence, most of the engine power is used for acceleration and steering during the backward movement. The lifting system in case a) maintains the same bucket height H to conserve energy in this period. When the loader is close to the unloading point, the wheel loader starts to decrease its speed and lift the bucket. As a result, the engine speed and output torque are kept within the fuel saving range, and driveline power loss is also reduced.

On the other hand, the energy conservation by the delay lifting strategy in case b) makes the wheel loader motion less sensitive to changes in elevation. The reversing point in case b), shown in 4, is 0.72 m higher than in case a). Due to the selected path in the backward movement, the speed profile in case b) is slower than case a) wheras the downhill path adopts faster speed in the forward movement. Although the delay lifting strategy leads to the highest production rate according to table II), the separated bucket lifting action resulted in more power loss than the integrated

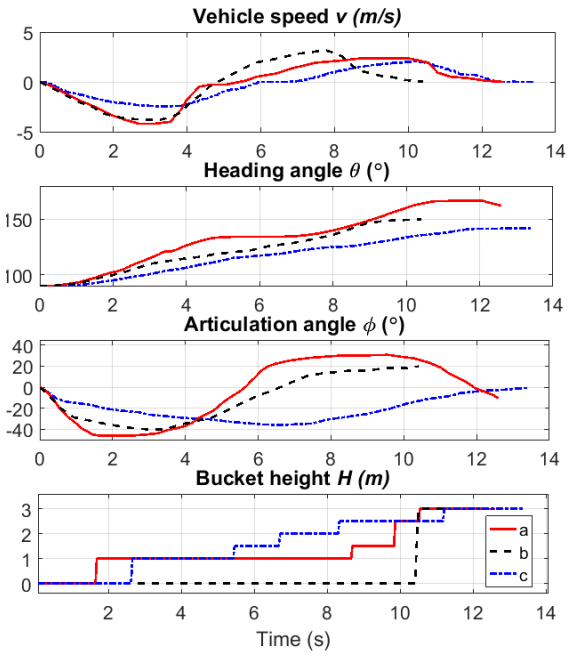

Figure 5. Comparison of optimal vehicle profiles. Initial conditions and state constraints are the same in all cases: maximum bucket load $m_{load} = 3$ ton, maximum terminal time $T_{max} = 14$ s, and BSFC limitation $\psi_{max} = 230$ mg/kWh.

Table II
RESULTS OF THE OPTIMAL LOADING CYCLE.

Cases	unit	**a**	**b**	**c**
Terrain info	–	3D	3D	2D
Trajectory length	*m*	22.39	21.67	27.18
Time	s	12.36	10.34	13.75
BSFC	*mg/kWh*	184	190	221
Production rate	*ton/s*	0.242	0.279	0.218
Energy loss rate	%	16.4	19.5	22.3
Fuel consumption	*g*	10.51	11.75	12.87

loading strategy. The reason is that the bucket is straightly lifted after the vehicle arrives at its final position, and the increasing speed ratio between engine and vehicle n_e/v will cause more power loss in the driveline system. When 2D optimal path is implemented in the construction site without considering terrain information, more energy is required than operating on a flat terrain and the optimal power balance inside drivenline cannot be maintained. As a result, the fuel consumption is 13.4% higher than operating the loader on a completely flat site.

In summary, the loading trajectory shows strong sensitivity to the change of construction site terrain. Optimizing loading path and applying different lifting strategies could facilitate the improvement of energy efficiency.

V. SUMMARY AND FUTURE WORK

This paper has proposed a path optimization approach for wheel loader in construction site. One extension of the early study is the involvement of terrain information in path planning. The vehicle dynamic model is extended to the 3D case with simplification and bucket height is also explicitly modeled. Compared to the 2D vehicle model, the state and control are even more complex. While the path optimization approach is established based on an optimal control framework, a grid-base search method is developed based on the solution approach for discrete dynamic programming. The computational efficiency is significantly enhanced from the early work by parallel searching on both forward and backward movements. The numerical experiments investigate the effects of construction site terrain and lifting strategies in term of fuel consumption, production rate, and energy efficiency. The simulation results show that the presented path optimization approach is capable of doing motion planning for wheel loader in a 3D environment.

The current work has not considered emissions of wheel loader. For more sustainable transport and construction, this should be added as an additional criteria for optimization. In the mean time, the computational cost for the proposed approach is still high for engineering application. The future work should focus on further enhancing the computational efficiency.

REFERENCES

[1] T. Samuelsson, R. Filla, B. Frank, and L. Skogh, "Selecting representative working cycles from large measurement data sets," *CVT 2016 Commercial Vehicle Technology Symposium*, 2016.

[2] B. Paden, M. Čáp, S. Z. Yong, D. Yershov, and E. Frazzoli, "A survey of motion planning and control techniques for self-driving urban vehicles," *IEEE Transactions on Intelligent Vehicles*, vol. 1, no. 1, pp. 33–55, 2016.

[3] J.-w. Choi and K. Huhtala, "Constrained global path optimization for articulated steering vehicles," *IEEE Transactions on Vehicular Technology*, vol. 65, no. 4, pp. 1868–1879, 2016.

[4] T. Berglund, A. Brodnik, H. Jonsson, M. Staffanson, and I. Soderkvist, "Planning smooth and obstacle-avoiding b-spline paths for autonomous mining vehicles," *IEEE Transactions on Automation Science and Engineering*, vol. 7, no. 1, pp. 167–172, 2010.

[5] B. Alshaer, T. Darabseh, and M. Alhanouti, "Path planning, modeling and simulation of an autonomous articulated heavy construction machine performing a loading cycle," *Applied Mathematical Modelling*, vol. 37, no. 7, pp. 5315–5325, 2013.

[6] T. Nilsson, A. Fröberg, and J. Åslund, "Predictive control of a diesel electric wheel loader powertrain," *Control Engineering Practice*, vol. 41, pp. 47–56, 2015.

[7] V. Nezhadali and L. Eriksson, "Optimal lifting and path profiles for a wheel loader considering engine and turbo limitations," in *Optimization and Optimal Control in Automotive Systems*. Springer, 2014, pp. 301–324.

[8] V. Nezhadali, B. Frank, and L. Eriksson, "Wheel loader operation - optimal control compared to real drive experience," *Control Engineering Practice*, vol. 48, pp. 1–9, 2016.

[9] B. Hong and X. Ma, "Path planning for wheel loaders: a discrete optimization approach," in *20th IEEE International Conference on Intelligent Transportation Systems*. IEEE, 2017.

[10] S. El-Omari and O. Moselhi, "Integrating 3d laser scanning and photogrammetry for progress measurement of construction work," *Automation in construction*, vol. 18, no. 1, pp. 1–9, 2008.

[11] S. Siebert and J. Teizer, "Mobile 3D mapping for surveying earthwork projects using an unmanned aerial vehicle system," *Automation in Construction*, vol. 41, pp. 1–14, 2014.

[12] B. Hong, X. Ma, H. Chen, and L. Lv, "Modeling of dynamic NOx emission for nonroad machinery: a study on wheel loader using engine test data and on-board measurement," in *Transportation Research Board 95th Annual Meeting, Washington D.C.*, 2016.